BIOCHEMISTRY
including biophysical chemistry & molecular biology

Article

pubs.acs.org/biochemistry

# Primary Photodynamics of the Green/Red-Absorbing Photoswitching Regulator of the Chromatic Adaptation E Domain from *Fremyella diplosiphon*

Sean M. Gottlieb,[†] Peter W. Kim,[†] Nathan C. Rockwell,[‡] Yuu Hirose,[§] Masahiko Ikeuchi,[§,∥] J. Clark Lagarias,[‡] and Delmar S. Larsen*[,†]

[†]Department of Chemistry, University of California, One Shields Avenue, Davis, California 95616, United States

[‡]Department of Molecular and Cell Biology, University of California, One Shields Avenue, Davis, California 95616, United States

[§]Electronics-Inspired Interdisciplinary Research Institute, Toyohashi University of Technology, 1-1 Hibarigaoka Tempaku, Toyohashi, Aichi 441-8580, Japan

[∥]Department of Life Sciences, University of Tokyo, 3-8-1 Komaba, Meguro-ku, Tokyo 153-8902, Japan

Supporting Information

**ABSTRACT:** Phytochromes are red/far-red photosensory proteins that utilize the photoisomerization of a linear tetrapyrrole (bilin) chromophore to detect the red to far-red light ratio. Cyanobacteriochromes (CBCRs) are distantly related cyanobacterial photosensors with homologous bilin-binding GAF domains, but they exhibit greater spectral diversity. Different CBCR subfamilies have been described, with spectral sensitivity varying across the near-ultraviolet and throughout the visible spectrum, but all known CBCRs utilize photoisomerization of the bilin 15,16-double bond as the primary photochemical event. The first CBCR discovered was RcaE, responsible for tuning light harvesting to the incident color environment (complementary chromatic adaptation) in *Fremyella diplosiphon*. The green/red RcaE photocycle has recently been described in detail. We now extend this analysis by examining femtosecond photodynamics using ultrafast transient absorption techniques with broadband detection and multicomponent global analysis. Excited-state dynamics in both directions are significantly slower than those recently published for the red/green CBCR NpR6012g4. In the forward reaction, the primary Lumi-G photoproduct arises from the longer-lived excited-state populations, leading to a low photoproduct quantum yield. Using dual-excitation wavelength interleaved pump−probe spectroscopy, we observe multiphasic excited-state dynamics in the forward reaction ($^{15Z}P_g \rightarrow {}^{15E}P_r$), which we interpret as arising from ground-state inhomogeneity with different tautomers of the PCB chromophore. The reverse reaction ($^{15E}P_r \rightarrow {}^{15Z}P_g$) is characterized via pump−probe spectroscopy and also exhibits slow excited-state decay dynamics and a low photoproduct yield. These results provide the first description of excited-state dynamics for a green/red CBCR.

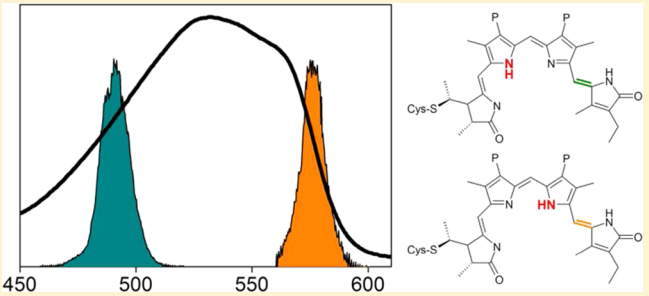


Photosensory proteins allow organisms to respond to the ambient light environment through behaviors such as phototaxis, optimization of the photosynthetic apparatus for ambient color and intensity, and regulation of gene expression.[1−4] Several families of photoreceptors have been identified with sensitivity in the blue region of the spectrum; responses to longer wavelengths are associated with phytochromes. Phytochromes were first identified as critical regulators of photomorphogenesis and shade avoidance in plants and have been subsequently discovered in bacteria, cyanobacteria, and fungi.[2,4,5] Phytochromes exhibit a conserved photosensory core, including a GAF domain that binds the linear tetrapyrrole (bilin) chromophore.[4,5] Photoexcitation of the bilin initiates reversible isomerization of the 15,16-double bond (Figure 1) to photoconvert between dark-stable, red-absorbing $P_r$ and metastable far-red-absorbing $P_{fr}$ photostates.[4−7]

The bilin-binding GAF domain of phytochromes is shared by cyanobacteriochromes (CBCRs), a distantly related family of cyanobacterial photosensors.[4,5,8] CBCRs differ widely in spectral response, with different classes exhibiting spectral sensitivities spanning the entire visible spectrum, but C15,16 photoisomerization remains the primary photochemical event.[4,9−14] The first CBCR to be discovered was RcaE, which regulates complementary chromatic adaptation (CCA) in the filamentous cyanobacterium *Fremyella diplosiphon*.[15,16] RcaE photoswitches between a green-absorbing $^{15Z}P_g$ dark state and a red-absorbing $^{15E}P_r$ photoproduct in a green/red photocycle (Figure 1). Green/red CBCRs such as RcaE,

**Received:** July 16, 2013
**Revised:** October 18, 2013
**Published:** October 23, 2013





dx.doi.org/10.1021/bi400946q | *Biochemistry* 2013, 52, 8198−8208

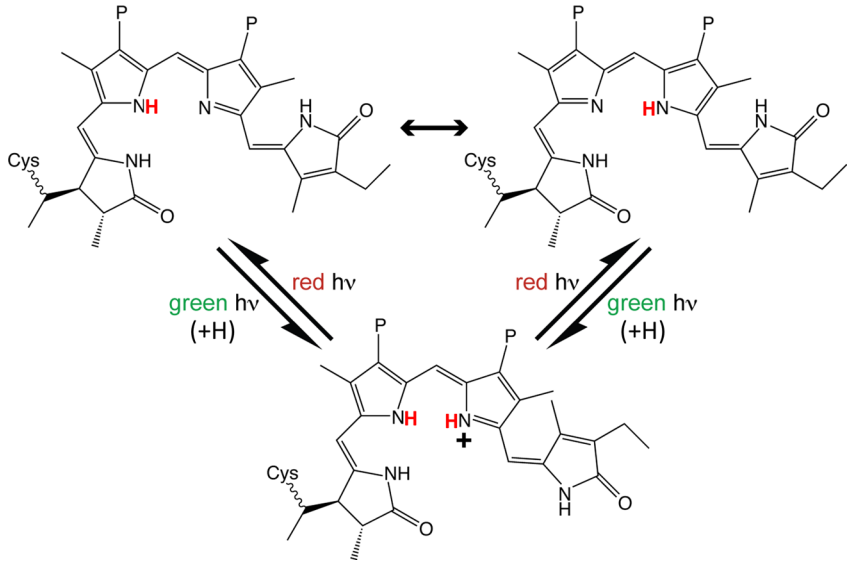


**Figure 1.** Protochromic photocycle of RcaE. In this photocycle, the phycocyanobilin (PCB) chromophore exhibits a deprotonated, green-absorbing $^{15Z}P_g$ dark state and a protonated, red-absorbing $^{15E}P_r$ photoproduct. Two tautomers are possible for PCB in the $^{15Z}P_g$ state. P indicates propionate.

SyCcaS, and NpCcaS exhibit a protochromic photocycle, with the bilin ring system of $^{15Z}P_g$ being deprotonated and that of $^{15E}P_r$ being protonated; proton transfer is essential for generating the spectral separation between the green- and red-absorbing states.[16−18]

Interestingly, there is also a large family of CBCRs that exhibit the reverse photocycle, in which a red-absorbing dark state ($^{15Z}P_r$) photoconverts to a metastable green-absorbing $^{15E}P_g$ photoproduct.[14,19,20] Although less is known about the mechanistic basis for this red/green photocycle, the femtosecond photodynamics of one such protein, NpR6012g4 from *Nostoc punctiforme*, have been characterized in detail.[20−22] For NpR6012g4, both the forward ($^{15Z}P_r \rightarrow {}^{15E}P_g$) and reverse ($^{15E}P_g \rightarrow {}^{15Z}P_r$) reaction dynamics exhibit unusually high photoisomerization quantum yields (Φ values of ∼40−50%) relative to those of phytochromes (Φ values of <15%).[23−26] Both the $^{15Z}P_r$ and $^{15E}P_g$ states of NpR6012g4 have been modeled as heterogeneous.[20−22] For $^{15Z}P_r$, this interpretation is further supported by static measurements implicating the presence of multiple subpopulations with similar peak wavelengths and line shapes, but varying extinction coefficients and/or photochemical quantum yields.[14] Heterogeneity was directly demonstrated for the $^{15E}P_g$ photostate of NpR6012g4 using a dual-excitation-wavelength interleaved (DEWI) pump−probe approach.[22] Similar analyses have not been reported for green/red CBCRs such as RcaE.

Here, we describe the femtosecond to nanosecond photodynamics of recombinant RcaE for both forward and reverse photoreactions. Quantum yields are much lower than those of NpR6012g4. For the forward reaction ($^{15Z}P_g \rightarrow {}^{15E}P_r$), transient signals were measured using DEWI pump-probe to resolve the spectral and dynamic characteristics of any underlying excitation wavelength dependence with subsequent global analysis. Multiphasic excited-state dynamics were observed, which were interpreted as arising from ground-state inhomogeneity of $^{15Z}P_g$. This work presents the first ultrafast examination of a green/red CBCR, revealing considerable differences relative to the "reversed" red/green CBCR NpR6012g4.

## MATERIALS AND METHODS

**Protein Expression, Purification, and Static Characterization.** The GAF domain of RcaE was purified from PCB-producing *Escherichia coli* cells exactly as described previously.[16] Absorption spectra were acquired on a Cary 50 spectrophotometer, and static fluorescence spectra were acquired on a PTI QM-6/2005SE fluorometer equipped with red-enhanced photomultiplier tubes.

**Ultrafast Transient Absorption Spectroscopy.** The broadband transient absorption setup was constructed from an amplified Ti:sapphire laser system (Spectra Physics Spitfire Pro and Tsunami) operating at 1 kHz that produced 2.25 mJ pulses of 800 nm fundamental output with a 40 fs full width at half-maximum duration.[27] The fundamental pulse train from the amplifier was split into multiple paths with one path generating the dispersed supercontinuum probe pulses (425−725 nm) by focusing the 800 nm pulses into a slowly translating 2 mm thick $CaF_2$ crystal. Two separate paths were used to generate tunable visible pulses from separate home-built noncollinear optical parametric amplifiers (NOPAs) as excitation/pump sources (490 and 575 nm) for resolving the DEWI wavelength dependence of the forward reaction ($^{15Z}P_g \rightarrow {}^{15E}P_r$) dynamics (Figure 2). Both 490 and 575 nm pump beams were mechanically chopped to generate a pulse sequence with the reference and excited spectra collected sequentially. The collection of DEWI pump−probe signals minimizes possible errors caused by long-term fluctuations in excitation power, sample degradation, and different experimental conditions and constitutes the best possible approach to identifying the excitation wavelength dependence of transient absorption signals.[22,28] For the reverse reaction ($^{15E}P_r \rightarrow {}^{15Z}P_g$) kinetics, excitation pulses at 650 nm were generated by a single NOPA (Figure 2); no DEWI signals were collected for the reverse reaction dynamics.

The broadband probe beam was optically delayed with respect to the pump pulses by a computer-controlled linear motor stage (Newport model IMS600LM), which allowed a temporal range of up to 7 ns. The pump pulses were linearly polarized at 54.7° (magic angle) with respect to the probe pulses, and the ∼300 μm pump and 50 μm probe spot


dx.doi.org/10.1021/bi400946q | *Biochemistry* 2013, 52, 8198−8208

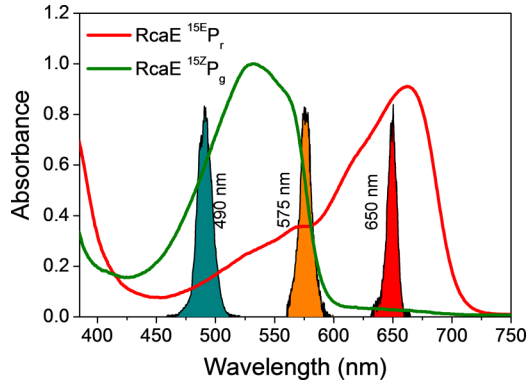


**Figure 2.** Ground-state absorption spectra of the $^{15Z}P_g$ and $^{15E}P_r$ states of RcaE. Ground-state $^{15Z}P_g$ absorption spectrum (green curve) shown with 490 nm (cyan area) and 575 nm (orange area) pump pulse spectra used for the DEWI pump−probe experiment. Ground-state $^{15E}P_r$ absorption spectrum (red curve) shown with the 650 nm (red area) pump pulse spectrum used for the pump−probe experiment.

diameters were estimated using a micrometer stage and razor blade; the larger pump pulse diameter minimizes artifactual contributions to the signals from a varying spatial overlap between pump and probe beams. This was confirmed by monitoring the signal amplitude and spectral shape when dithering the pump beam with respect to the probe beam. The uniform decay of the full transient spectrum when dithering this spatial overlap indicates that no spatial-dependent deviations exist between the pump and probe beams and ensures that the two simultaneously collected DEWI transient absorption signals can be directly compared.

The 150 fs temporal resolution of the signals (both forward and reverse reactions) was estimated from the rise of the ESA bands. For the forward reaction experiment, the sample was flowed continuously in a closed circuit to ensure fresh sample for each excitation pulse and was continuously illuminated in an ∼1 cm cell with 20 mW of 660 nm LED light (Epitex Inc. model L660-66-60) through a glass window in the sample flow line to cycle the proteins to the desired $^{15Z}P_g$ state prior to ultrafast interrogation in a separate 2 mm cuvette. For the reverse reaction, the sample was similarly illuminated with 20 mW of 525 nm LED light (Epitex Inc. model L525-66-60) to cycle the sample to the $^{15E}P_r$ state. The optical density at the primary absorption peak was ∼0.3 per 2 mm cuvette, and all experiments were conducted at 25 °C.

**Global Analysis.** The transient signals were analyzed within a multicompartment global analysis formalism that fits the data to an underlying "target" model with time-dependent populations (concentration profiles) attributed with time-independent spectra [species-associated difference spectra (SADS)].[29,30] This was accomplished by fitting the data with numerical solutions of linear first-order differential equations describing a postulated model (eq 1):

$$\frac{dn_i}{dt} = A_i I(t) + \sum_j K_{ij} n_j \quad (1)$$

where $n_i$ represents the microscopic population of interest, $A_i$ is the initial population of the $i$th excited state, $I(t)$ is the pump pulse temporal width, and $K$ is the rate constant matrix that describes the exponential flow of one population into another. If the underlying target model accurately describes the dynamics, the extracted spectra from the analysis are called SADS and represent the true difference spectra of the constituent populations. If the model inaccurately describes the dynamics, the resulting spectra from the global fitting are evolution-associated difference spectra (EADS) and represent linear combinations of the underlying SADS.[20,29,30] For all data sets, a sequential EADS model was first used to estimate the underlying "apparent" (i.e., experimentally observed) time scales in the data. Although this approach adequately fits the data with EADS with increasing lifetimes, it does not decompose the apparent time scales into the microscopic time scales describing the evolution of microscopic populations, which are estimated with more sophisticated target analyses.[20,29,30]

## RESULTS

**Forward Reaction Dynamics ($^{15Z}P_g \rightarrow {}^{15E}P_r$).** The $^{15Z}P_g$ ground-state absorption spectrum (Figure 2) is distinctly non-Gaussian, with a primary peak at 530 nm and a shoulder at 570 nm. DEWI pump−probe spectra were recorded with 490 and 575 nm excitation pulses under otherwise identical experimental conditions to evaluate potential wavelength dependence in the ultrafast dynamics. Spectra taken with either pump pulse are contrasted in Figure 3 at selected probe times. Such

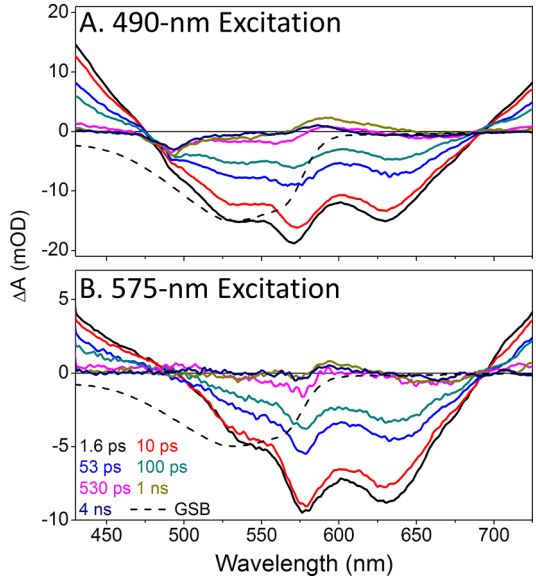


**Figure 3.** Transient DEWI spectra of the forward dynamics of (A) 490 nm excitation data and (B) 575 nm excitation data at selected probe times indicated in the legend. The inverted $^{15Z}P_g$ ground-state absorption band is overlaid as a visual aid (−−−).

transient spectra arise from four overlapping contributions: (1) negative ground-state bleach (GSB) resulting from the loss of absorbance by the reduced ground-state population, (2) positive excited-state absorptions (ESAs) resulting from the transitions into higher-lying electronic states ($S_1 \rightarrow S_n$), (3) negative stimulated emission (SE) resulting from de-excitation of the excited-state species by the probe pulse ($S_1 \rightarrow S_0$), and (4) positive absorption arising from structurally evolved ground-state photoproduct species, which is shifted relative to the initial negative ground-state absorption due to the structural evolution initiated by excitation.

The two DEWI data sets exhibit qualitatively similar spectral features (Figure 3): transient spectra at 1.6, 10, 53, and 100 ps exhibit two distinct SE bands near 570 and 630 nm with


dx.doi.org/10.1021/bi400946q | Biochemistry 2013, 52, 8198−8208

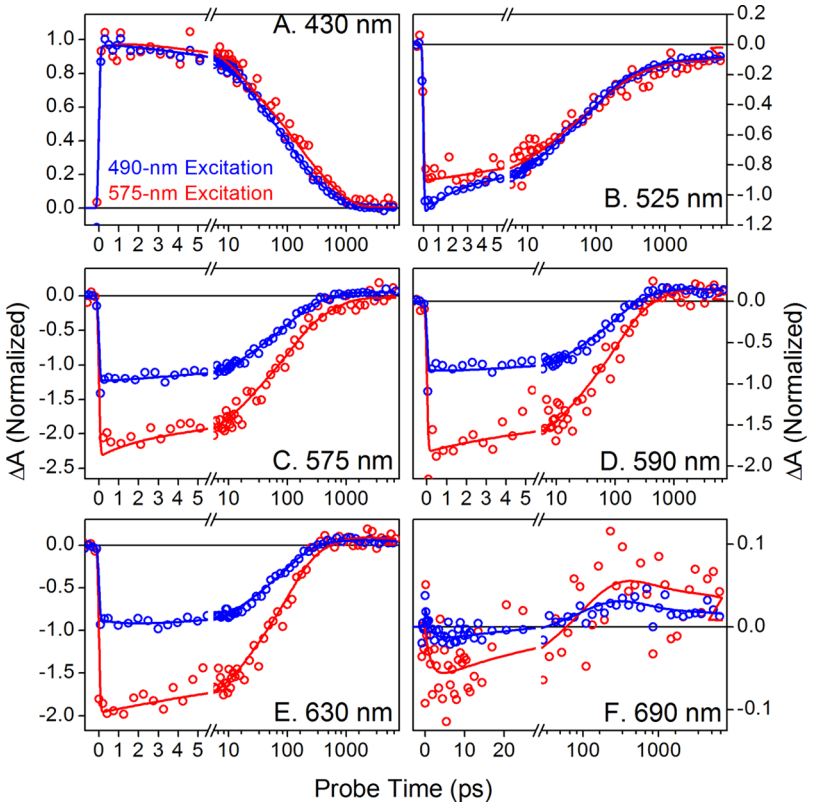


**Figure 4.** Kinetic traces of the forward reaction at selected probe wavelengths for 490 nm (blue circles) and 575 nm (red circles) excitation data. Each kinetic trace is scaled to the normalized 430 nm amplitude for comparison. Each kinetic trace is fit with the sequential model (blue curve for 490 nm excitation and red curve for 575 nm excitation).

positive ESA bands observed at both ends of the spectral window. The two SE bands correspond to resolvable bands in the fluorescence emission spectrum (Figure S1 of the Supporting Information). The excited-state populations ($P_g$*) decay within 1−2 ns (Figure 3, light brown curves) and are more clearly resolved at 430 nm (Figure 4A) with minimal contributions from the GSB and SE (Figure 3). A new positive 590 nm absorption develops within ∼500 ps in both data sets (Figure 3, magenta curves), corresponding to the primary photoproduct, $^{15E}$Lumi-$G_1$. This absorption band continues to grow to 1 ns before a second photoproduct, $^{15E}$Lumi-$G_2$, is formed (Figure 3, magenta, light brown, and purples curves). $^{15E}$Lumi-$G_2$ is long-lived and is blue-shifted relative to Lumi-$G_1$. A similar Lumi-$G_1$ → Lumi-$G_2$ evolution was observed in NpR6012g4.[22]

Although the DEWI data sets have qualitatively similar spectral features, they do exhibit distinct kinetic and spectral qualities (Figure 5). For 490 nm excitation, 50% of $P_g$* has decayed to the ground state within 75 ps and nearly 95% has decayed to the ground state within 1 ns. Excited-state decay is slower for 575 nm excitation, with 50% decay at 100 ps and nearly 95% decay at 2 ns. There are also slight differences at longer times [>1 ns (Figure 4)]. The $^{15E}$Lumi-$G_2$ primary photoproduct is metastable and partially fills the $P_g$ GSB before evolving to the next step in the photodynamics beyond the time frame of this experiment; such instability of the primary photoproduct has not been reported for phytochrome or CBCR systems to date. Spectrally, the GSB exhibits a clear wavelength dependence. This can readily be seen by comparing the relative amplitudes of the GSB peak at 525 nm and the SE band peak at 575 nm: the amplitude of the GSB peak is greater

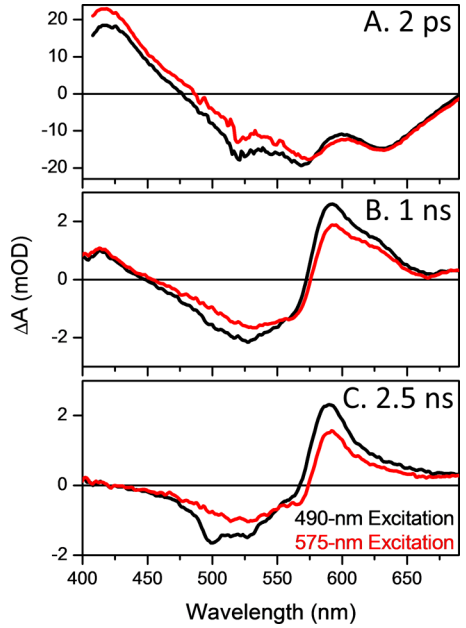


**Figure 5.** Transient spectra are shown for individual probe times with high averaging (20 times more than Figure 3) to allow an increased signal-to-noise ratio at the expense of reduced time resolution. All spectra are normalized to the SE band at 630 nm and at the 2 ps probe time. Under this normalization, comparison of the two excitation wavelengths at 1 and 2.5 ns shows the difference in quantum yield as lower magnitudes for the positive Lumi-G bands upon 575 nm excitation, albeit with spectrally identical Lumi-G features.


dx.doi.org/10.1021/bi400946q | *Biochemistry* 2013, 52, 8198−8208

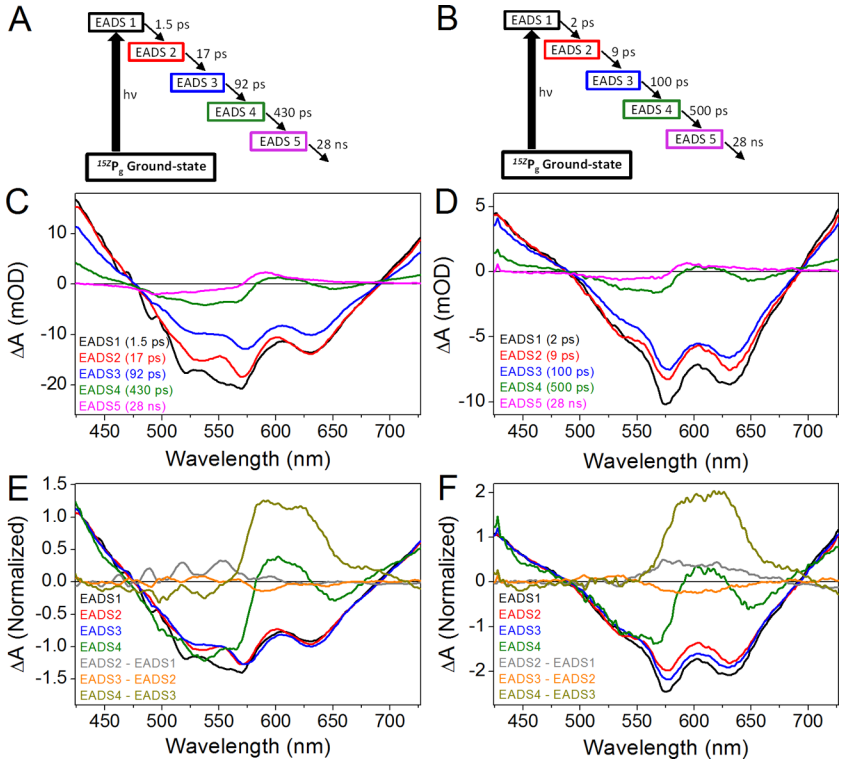


**Figure 6.** Global analysis of the (A, C, E) 490-nm and (B, D, F) 575-nm excitation forward reaction data with five component sequential models (A and B). (C and D) Evolution-associated difference spectra (EADS) with time constants for each spectrum in the legend. (E and F) EADS1, -2, and -3 normalized at the ESA regions, with the normalized EADS2 − EADS1 (dark gray) and normalized EADS3 − EADS2 (light gray) differences shown to demonstrate the spectral evolution between the EADS is independent of excited-state decay.

**Table 1. Forward, $^{15Z}P_g \rightarrow {}^{15E}P_r$, Inhomogeneous Target Analysis Parameters**

| | ESI1 | ESI2 | ESI3 | $^{15E}$Lumi-$G_1$ | $^{15E}$Lumi-$G_2$ |
|---|---|---|---|---|---|
| initial occupancy (%) (490 nm excitation) | 25 | 55 | 20 | 0 | 0 |
| initial occupancy (%) (575 nm excitation) | 25 | 44 | 31 | 0 | 0 |
| $\tau_{effective}$ | 15 ps | 100 ps | 510 ps | 500 ps | 10 ns (3.5 ns) |
| $\tau$ | 15 ps (GS1) | 130 ps (GS2), 450 ps ($^{15E}$Lumi-$G_1$) | 560 ps (GS3), 6 ns ($^{15E}$Lumi-$G_1$) | 230 ps ($^{15E}$Lumi-$G_2$) | – |
| branching yield | 100% (GS1) | 78% (GS2), 22% ($^{15E}$Lumi-$G_1$) | 91% (GS3), 9% ($^{15E}$Lumi-$G_1$) | 100% ($^{15E}$Lumi-$G_2$) | – |
| $^{15E}$Lumi-$G_1$ Φ (%) (490 nm) | 0 | 12 | 2 | – | – |
| $^{15E}$Lumi-$G_1$ Φ (575 nm) | 0 | 10 | 3 | – | – |

than that of the SE band at 490 nm excitation than at 575 nm excitation.

To extract the apparent time scales from the DEWI data, we initially performed global analysis independently on the 490 and 575 nm excitation transient data sets using a sequential model. This approach allows extraction of sequential EADS as a first step in building a target model.[20] Sequential analyses of the DEWI-PP data sets are presented in Figure 6. Both data sets required five populations to adequately fit the data. The 575 nm excitation data were fit with time constants of 2 ps, 9 ps, 100 ps, 500 ps, and 28 ns (Figure 6B). The first three EADS exhibit features of the electronic excited state ($P_g$*), with clearly resolved ESA and SE signals (Figure 6D). EADS4 demonstrates a significant depletion of the $P_g$* population and an increase in the level of the 600 nm $^{15E}$Lumi-$G_1$ photoproduct. To separate spectral evolution from population decay in the signals, we normalized the EADS1, EADS2, and EADS3 at the 630 nm SE band and then generated EADS2 − EADS1 and EADS3 − EADS2 difference spectra for comparison (Figure 6F). The first three EADS were spectrally nearly identical aside from their amplitudes, with no discernible spectral evolution resolved within the signal-to-noise ratio of the data. Therefore, $^{15E}$Lumi-$G_1$ is not generated from the 100 ps $P_g$* population.

The raw data show that 490 nm excitation resulted in a greater apparent $^{15E}$Lumi-$G_1$ amplitude than did excitation at 575 nm (Figure 5). However, the peak wavelength and line shape of $^{15E}$Lumi-$G_1$ were independent of excitation wavelength, so this difference either indicates generation of multiple products differing only in their extinction coefficients or generation of a single product from both excitation wavelengths, with a wavelength-dependent photochemical quantum yield of Φ. For reasons discussed below, the latter interpretation is favored; under this assumption, we were able to estimate the Φ of $^{15E}$Lumi-$G_2$ to be 14% for 490 nm excitation and 12.5% for 575 nm excitation (Table 1).

The features of the forward reaction EADS indicate that the underlying dynamics induced after excitation of the $^{15Z}P_g$ state of RcaE are complex and involve multiple populations (both


dx.doi.org/10.1021/bi400946q | Biochemistry 2013, 52, 8198−8208

excited-state and ground-state) that evolve with strong spectral and temporal overlap. A simple decomposition of the transient data into separate co-evolving populations with excitation wavelength-dependent occupations requires improved TA data and likely new experimental approaches (e.g., pump−dump−probe) to identify a proper model with clearly resolved populations. Despite this, two preliminary target models have been attempted with the $^{15E}$Lumi-G$_1$ and $^{15E}$Lumi-G$_2$ intermediates evolving sequentially (Figure S2 of the Supporting Information) or in parallel (Figure S3 of the Supporting Information). Unfortunately, these models were unable to spectrally compose the estimated SADS into excitation wavelength-dependent pathways despite the obvious differences in the DEWI data (Figures 3−6).

**Reverse Reaction ($^{15E}$P$_r$ → $^{15Z}$P$_g$).** The ground-state absorption of $^{15E}$P$_r$ peaks at 660 nm with two prominent shoulders at 620 and 575 nm (Figure 2, solid red line). Selected transient spectra for the reverse photoreaction are shown in Figure 7 after 650 nm excitation. Transient spectra at <100 ps

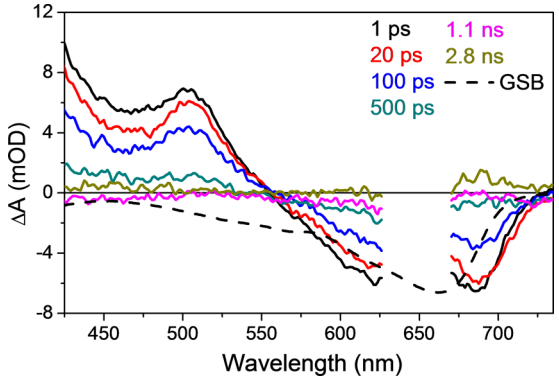


**Figure 7.** Transient spectra of the reverse reaction excited with 650 nm at select probe delay times, as specified in the legend. The inverted $^{15E}$P$_r$ ground-state absorption spectrum (−−−) is overlaid as a visual guide.

exhibit positive ESA bands at <500 nm and two negative bands at 620 and 680 nm, which are superpositions of GSB, ESA, and SE. The SE band resembles the fluorescence spectrum of P$_r$* (Figure S1 of the Supporting Information) and exhibits a rapid slight red shift (Figure S7 of the Supporting Information). At later times, these signals undergo a transition into a low-amplitude positive population absorbing at 690 nm. This population persists to the experimental limit (>7 ns) without decay and is attributed to the $^{15Z}$Lumi-R photoproduct. The P$_r$* decay kinetics at select probe wavelengths are contrasted in Figure 8. The 515 nm kinetics track ESA decay, while the 606 nm kinetics track GSB decay and 693 nm kinetics SE (overlapped with probable ESA and GSB) and subsequent $^{15Z}$Lumi-R formation (Figure 7, 2.8 ns). The weak $^{15Z}$Lumi-R signals are consistent with the low quantum yield for the reverse direction.

Three decay components (60 ps, 375 ps, and ∞) are needed in the sequential EADS analysis to fit the reverse reaction signals (Figure 9). EADS1 and EADS2 share similar spectra and are nearly identical after normalization at the ESA band near 500 nm (Figure 9C). There is, however, deviation in the red region of the normalized EADS1 and EADS2, which appears to red shift the SE band (>680 nm) and is consistent with the raw data (Figure S7 of the Supporting Information). The EADS2 −

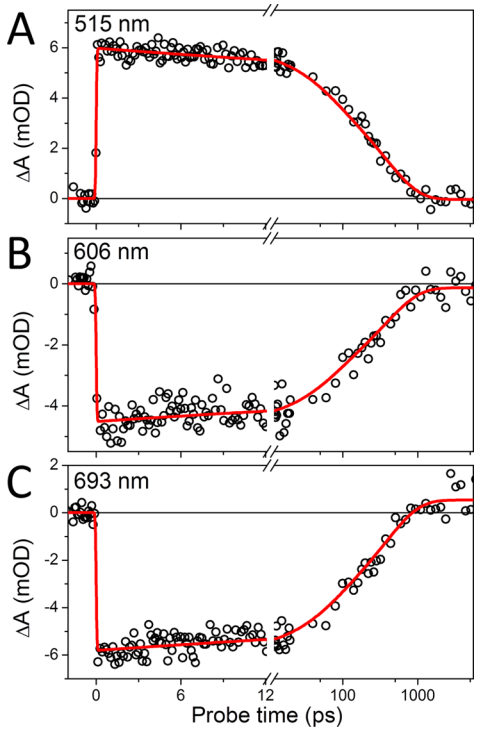


**Figure 8.** Kinetic traces of the reverse, $^{15E}$P$_r$ → $^{15Z}$P$_g$, reaction. Data plotted with fits extracted from the target model (Figure 12). Kinetic traces of the ESA band at (A) 515 nm and GSB and SE bands at (C) 606 nm and (D) 693 nm, respectively. The 693 nm kinetic trace tracks the growth of the $^{15Z}$Lumi-R population.

EADS1 difference spectrum calculated after normalization also shows this red shift. The nearly identical EADS1 and EADS2 suggest that $^{15Z}$Lumi-R is not generated from the faster 60 ps population, but from the slower 375 ps excited-state population. Consistent with this, the majority of the spectral evolution occurs between EADS2 and EADS3: the excited-state signals have decayed in EADS3, leaving the absorption band of the $^{15Z}$Lumi-R photoproduct peaking near 680 nm.

In contrast to the forward reaction dynamics, which are too complicated to adopt a viable target model, a feasible target model can be constructed to fit the reverse reaction data with the corresponding SADS and concentration profiles (Figure 10). This model is simpler than the forward reaction model and involves only two excited-state populations. A trial homogeneous model is also consistent with the data (Figure S8 of the Supporting Information), but we favor the heterogeneous model because of the frequent heterogeneity of CBCRs.[14,20−22,31,32] As with the two postulated forward reaction target models (Figures S2A and S3A of the Supporting Information), the multiexponential time constants of P$_r$* are posited to originate from two ground-state populations (GS1 and GS2) that generate distinct excited-state intermediate P$_r$* populations: ESI1 and ESI2. The longer-lived ESI2 ($\tau_{apparent}$ = 385 ps) is a productive excited-state population from which 14% is estimated to generate primary $^{15Z}$Lumi-R photoproduct (Table 2). Because the ESI2 population is estimated to be 70% of the total excited-state population, the total Φ of $^{15Z}$Lumi-R is estimated to be ∼10% (Table 2 and Figure 10B). The ESI SADS (Figure 10C, black and red curves) are nearly identical except for the small red-shifting SE dynamics (Figure S7 of the Supporting Information) and have comparable amplitudes (i.e., extinction coefficients).


dx.doi.org/10.1021/bi400946q | Biochemistry 2013, 52, 8198−8208

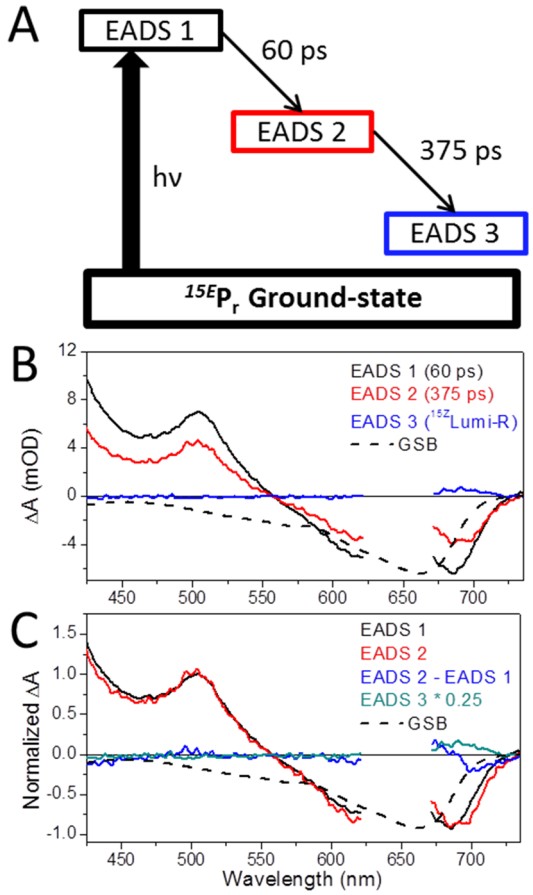


**Figure 9.** Sequential EADS analysis of the reverse reaction kinetics. (A) Three-component sequential model. (B) Evolution-associated difference spectra (EADS) with time constants for each spectrum in the legend. (C) Normalized EADS1 and EADS2 with respect to the ESA band at 500 nm, and the normalized EADS2 − EADS1 difference. The black dashed line is the inverted $^{15E}P_r$ ground-state spectrum to be used as a visual aid.

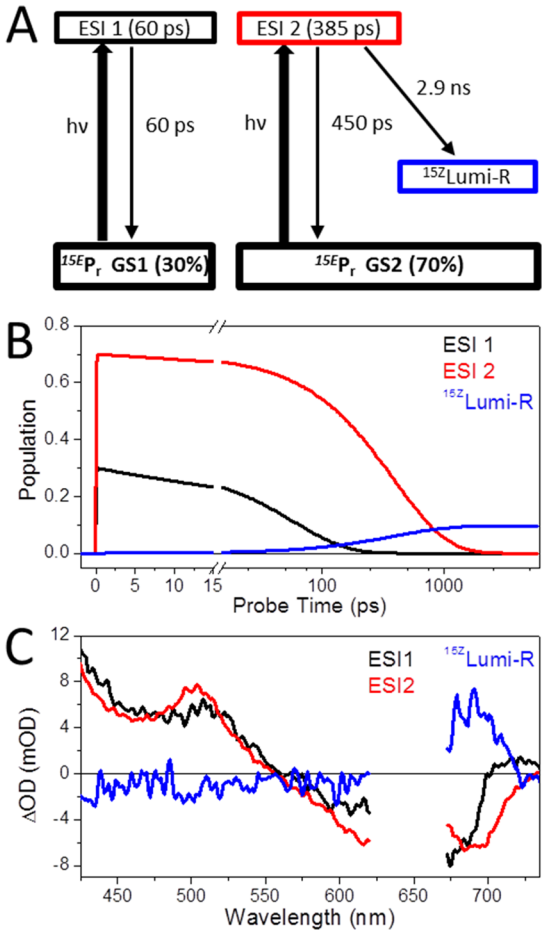


**Figure 10.** Target analysis of reverse reaction kinetics. (A) Inhomogeneous three-component decaying model used in target analysis. (B) Population profiles associated with the target model. (C) Species-associated difference spectra without constraining the first two excited-state species to the same spectrum. The black dashed curve is the inverted $^{15E}P_r$ ground-state spectrum to be used as a visual aid.

## DISCUSSION

We ascribe multiphasic excited-state dynamics in both the forward and reverse photoreactions of RcaE to ground-state heterogeneity (Figures S2 and S3 of the Supporting Information and Figure 10). For the forward reaction ($^{15Z}P_g \rightarrow {}^{15E}P_r$), this hypothesis is strongly supported by the excitation-dependent GSB bands (Figures 3, 5, and 6) observed in the DEWI pump−probe signals. Similar features were also observed in the DEWI signals of the reverse reaction ($^{15E}P_g \rightarrow {}^{15Z}P_r$) of NpR6012g4.[22] The static fluorescence spectrum of $^{15Z}P_g$ in RcaE is also highly dependent upon the excitation wavelength (Figure S9 of the Supporting Information), and the $^{15Z}P_g$ absorption and fluorescence spectra display clear evidence of inhomogeneous ground-state populations (Figure S1 of the Supporting Information). Both excited-state decay kinetics and $\Phi$ for generation of $^{15E}$Lumi-$G_1$ exhibited pronounced wavelength dependence, consistent with the heterogeneity of the static fluorescence spectra.

The ring system of $^{15Z}P_g$ is neutral and deprotonated.[16] This protonation state inherently allows ground-state inhomogeneity via tautomerization, with either the B or C ring being deprotonated (Figure 1). Upon excitation, $^{15Z}P_g$ undergoes photoisomerization about the C15=C16 bond to yield the $^{15E}$Lumi-$G_1$ and subsequent $^{15E}$Lumi-$G_2$ photoproducts. Proton transfer follows on a longer time scale to generate the final, fully protonated $^{15E}P_r$ photostate. In the SADS, the ground-state bleach bands of the $^{15E}$Lumi-$G_1$ photoproducts exhibit wavelength dependence (Figure 5). This indicates that equilibration of at least two ground-state subpopulations is slower on the ground-state surface than $^{15E}$Lumi-$G_1$ formation is on the excited-state surface [~0.5 ns (Figure 5)]. However, there is no such wavelength dependence in the photoproduct bands of the $^{15E}$Lumi-$G_1$ SADS (Figure S2 of the Supporting Information), indicating that equilibration of these two states is faster on the excited-state surface. In the RcaE pocket, the

**Table 2. Reverse, $^{15E}P_r \rightarrow {}^{15Z}P_g$, Inhomogeneous Target Analysis Parameters**

| | ESI1 | ESI2 | $^{15Z}$Lumi-R |
|---|---|---|---|
| initial occupancy (%) (650 nm) | 30 | 70 | 0 |
| $\tau_{effective}$ (ps) | 60 | 385 | – |
| $\tau$ | 60 ps (GS1) | 450 ps (GS2), 2.9 ns ($^{15Z}$Lumi-R) | – |
| branching yield | 100% (GS1) | 86% (GS2), 14% ($^{15Z}$Lumi-R) | – |
| $^{15Z}$Lumi-R yield (%) (650 nm) | 0 | ~10 | – |


dx.doi.org/10.1021/bi400946q | Biochemistry 2013, 52, 8198−8208

deprotonated 15*Z* state is maintained by the hydrophobic residue Leu249,[16] effectively creating a hydrophobic environment that favors the uncharged $\pi$ system. Such an environment would also retard tautomerization, because tautomerization would generate charge separation as the proton moves between nitrogen atoms. Excitation adds considerable energy to the system (~49 kcal/mol for a 575 nm photon), loosening the structure and allowing faster tautomerization. This interpretation thus provides a plausible working model for explaining the observed heterogeneity of the 15*Z* photostate of RcaE.

The fluorescence excitation spectra of RcaE exhibits pronounced wavelength dependence (Figure S9 of the Supporting Information), which is not consistent with equilibration of all populations on the excited-state surface. Therefore, there must be at least two subpopulations on the excited-state surface that are able to equilibrate on an ultrafast time scale, but also additional subpopulations that are unable to do so. We cannot resolve this additional complexity using currently available PP data with the EADS analysis or proposed target models (Figures S2 and S3 of the Supporting Information), which requires the application of PDP spectroscopy or similar multipulse techniques.

The ground-state inhomogeneity of $^{15Z}P_g$ RcaE is in agreement with a growing number of studies that support the presence of such inhomogeneity in phytochromes and CBCRs.[6,9,11,12,14,20−22,26,31−35] For example, a recent analysis of chromophore structure in the red/far-red phytochrome Cph1 using magic angle-spinning nuclear magnetic resonance revealed two ground-state isomers of the $P_r$ state, even though resonance Raman analysis of Cph1 instead suggests a homogeneous ground-state population.[6,25,36] Heterogeneity in CBCRs is less controversial: DXCF CBCRs such as Tlr0924 and TePixJ exhibit heterogeneous mixtures of PCB and phycoviolobilin, while the green-absorbing photostates of NpR6012g4 and RcaE exhibit clear wavelength dependence on an ultrafast time scale.[9,12,22,31]

Determining absolute Φ values from pump−probe data alone requires either knowledge of the extinction coefficient of the species in question or quantification of both the initial excited population and the final photoproduct population. The former approach is technically challenging for intermediates that themselves decay on a time scale of nanoseconds to microseconds. The latter approach requires a clean bleach band without overlapping ESA and SE bands, as has been demonstrated with PYP, RpBphP2, and RpBphP3.[26,37−40] However, there is no clean bleach region in the RcaE signals (Figures 3 and 7). The quantum yield for the forward reaction of NpR6012g4 was explicitly measured using pump−dump−probe techniques,[21] so we have used NpR6012g4 as a reference to generate an approximate Φ for RcaE. Both proteins convert between red- and green-absorbing states, albeit with a reversed configuration of the 15,16-double bond and markedly different excited decay kinetics (Figures 11C and 12C). Both proteins also give rise to spectrally similar primary photoproducts (Figures 11 and 12) and have similar green-absorbing extinction coefficients (44000 $M^{-1}$ $cm^{-1}$ for RcaE and 50000 $M^{-1}$ $cm^{-1}$ for NpR6012g4).[14] Therefore, it is plausible that the photoproduct extinction coefficients are also similar, making NpR6012g4 a reasonable reference to estimate Φ for RcaE in the same way that Cph1 was initially used as a reference for NpR6012g4 itself.[20,21] We therefore normalize the PP signals for the two proteins and used the resulting ratio of the final amplitudes for the two primary photoproducts to estimate Φ for RcaE from the known value for NpR6012g4.

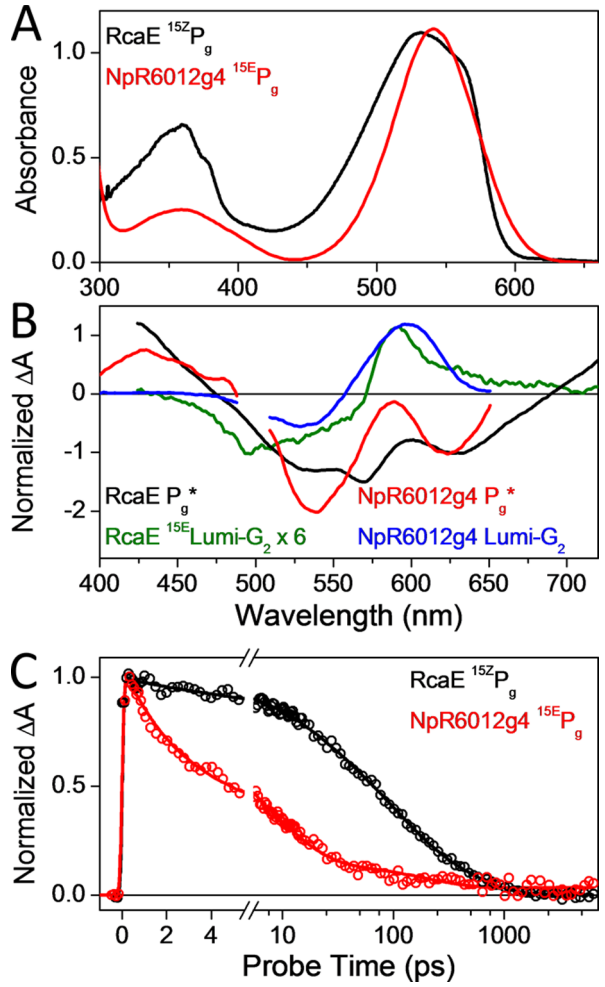


**Figure 11.** (A) Ground-state absorbance spectra of the $^{15Z}P_g$ state for RcaE (black) and NpR6012g4 (red) normalized at 540 nm. (B) Representative transient spectra of the initial $P_g$* state (EADS2 of sequential analysis of both RcaE and NpR6012g4) and final transient spectra of $^{15E}$Lumi-$G_2$ (EADS5 of sequential analysis), normalized at the SE band near 630 nm for EADS2 for both RcaE (black) and NpR6012g4 (red). The same normalizing factor was applied to the EADS5 spectra. (C) Kinetics of the excited state for RcaE (black circles) and NpR6012g4 (red circles) probed at the 430 nm ESA band.

The results of this procedure are shown in Figures 11B and 12B. For the $P_g \rightarrow P_r$ reaction (forward for RcaE and reverse for NpR6012g4 with 490 and 500 nm excitation, respectively, to allow normalization with comparable spectral regions), the initial $P_g$* signals were normalized at the SE band at 630 nm (Figure 11B). The corresponding $^{15E}$Lumi-$G_2$ amplitude of NpR6012g4 is approximately 6-fold greater than that of RcaE, suggesting a 6-fold lower Φ for RcaE (approximately 8−10%). For the $P_r \rightarrow P_g$ reaction (*E*/*Z* reverse for RcaE and *Z*/*E* forward for NpR6012g4), the initial $P_r$* is normalized at the clean ESA region near 500 nm (Figure 12B). The bleach and SE bands for RcaE after normalization, however, exhibit amplitudes lower than those of the bands of NpR6012g4, which could be due to a stronger ESA band overlapping the SE and GSB for RcaE.[22] Interestingly, the values of $P_r$* fluorescence of NpR6012g4 and RcaE are at similar peak wavelengths, but the SE band is smaller in RcaE (Figure 11B).


dx.doi.org/10.1021/bi400946q | *Biochemistry* 2013, 52, 8198−8208

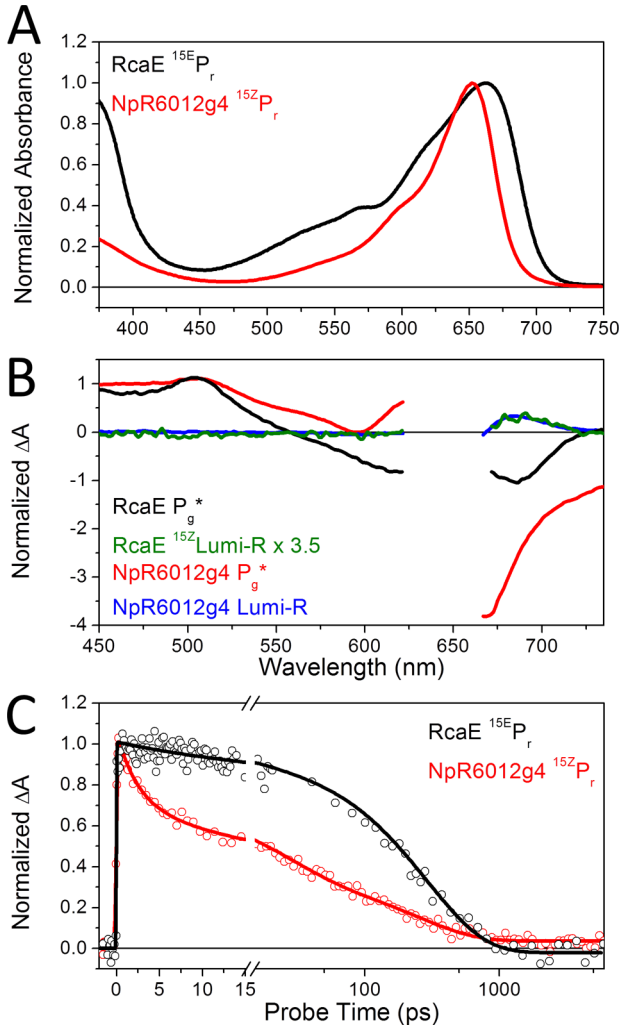


**Figure 12.** (A) Normalized ground-state absorbance spectra of $^{15E}P_r$ for RcaE (black) and NpR6012g4 (red). (B) Representative transient spectra of the initial $P_r$* state and final transient spectra of $^{15Z}$Lumi-R, normalized on the basis of the ESA bands near 500 nm for RcaE (black) and NpR6012g4 (red). This normalizing factor was applied to the $^{15Z}$Lumi-R spectra, where RcaE's $^{15Z}$Lumi-R was scaled by a factor of ~3.5. (C) Comparison of kinetics for the excited states of RcaE (black) and NpR6012g4 (red) probed at 500 nm, corresponding to ESA.

The $^{15Z}$Lumi-R spectra are nearly identical for RcaE and NpR6012g4, but the $^{15Z}$Lumi-R final amplitude of RcaE is ~3.5-fold smaller, implying a Φ for RcaE of approximately 11%. Thus, this procedure supports a lower Φ for RcaE than for NpR6012g4 in both reaction directions. This estimate is not a conclusive determination of the actual photoproduct Φ for RcaE. Pump−dump−probe techniques or others will be needed to address this question more rigorously.

Other green/red CBCRs have the conserved hydrophobic bilin-binding pocket and protochromic photocycle of RcaE,[16] so it is likely that a low Φ will be general for green/red CBCRs. The retention of green/red CBCRs as conserved CCA sensors in evolution despite the prevalence of more efficient red/green CBCRs like NpR6012g4 is an interesting point. Given the abundance of light-harvesting phycobiliproteins in the cyanobacterial cell and the energetic cost of remodeling this apparatus, it is possible that the low Φ of RcaE may prevent unstable "hair-trigger" responses to fluctuations in ambient light stimuli. However, it is also possible that the exceptional stability of green/red CBCRs across a broad pH range[16] is advantageous to organisms undergoing CCA in differing physical environments. Photosynthesis can produce changes in pH *in vivo*, so the ability of green/red CBCRs to lose photochromism at extreme pH values without irreversible loss of protein function may allow for a conserved role as integrators of two physiological cues: light and pH.

## ■ ASSOCIATED CONTENT

### Supporting Information

Static fluorescence emission and excitation spectra, proposed target models of the forward and reverse reaction dynamics, and a comparison of the DEWI EADS estimated from sequential analyses of the forward reaction dynamics. This material is available free of charge via the Internet at http://pubs.acs.org.

## ■ AUTHOR INFORMATION

### Corresponding Author

*E-mail: dlarsen@ucdavis.edu. Phone: (530) 754-9075.

### Author Contributions

S.M.G. and P.W.K. contributed equally to this work.

### Funding

This work was supported by grants from the Chemical Sciences, Geosciences, and Biosciences Division, Office of Basic Energy Sciences, Office of Science, U.S. Department of Energy (DOE DE-FG02-09ER16117), to both J.C.L. and D.S.L.

### Notes

The authors declare no competing financial interest.

## ■ ACKNOWLEDGMENTS

Dr. Mikas Vengris from Light Conversion Ltd. is acknowledged for the donation of the global and target analysis software package.

## ■ ABBREVIATIONS

CBCR, cyanobacteriochrome; CBD, chitin-binding domain; CCA, complementary chromatic adaptation; EADS, evolution-associated difference spectrum; SADS, species-associated difference spectra; ESI, excited-state intermediate; ESA, excited-state absorption; SE, stimulated emission; GAF, domain name derived from cGMP phosphodiesterase/adenylyl cyclase/FhlA; GSA, ground-state absorbance; RcaE, regulator of chromatic adaptation E; NOPA, noncollinear optical parametric amplifier; PAS, domain name derived from Per-ARNT-Sim; PΦB, phytochromobilin; PCB, phycocyanobilin; $P_r$, red-absorbing ground state of red/far-red phytochromes; $P_{fr}$, far-red-absorbing photoproduct state of red/far-red phytochromes; $^{15Z}P_r$, red-absorbing ground state of red/green CBCRs; Lumi-G, green-absorbing photoproduct state of red/green CBCRs; $P_g$*, excited-state population(s) derived from photoexcitation of $P_g$, also known as $^{15Z}P_g$; PYP, photoactive yellow protein; Φ, photocycle quantum yield.

## ■ REFERENCES

(1) Hoff, W. D., van der Horst, M. A., Nudel, C. B., and Hellingwerf, K. J. (2009) Prokaryotic phototaxis. *Methods Mol. Biol. 571*, 25−49.

(2) Franklin, K. A., and Quail, P. H. (2010) Phytochrome functions in *Arabidopsis* development. *J. Exp. Bot. 61*, 11−24.

(3) Möglich, A., Yang, X., Ayers, R. A., and Moffat, K. (2010) Structure and function of plant photoreceptors. *Annu. Rev. Plant Biol. 61*, 21−47.
(4) Auldridge, M. E., and Forest, K. T. (2011) Bacterial phytochromes: More than meets the light. *Crit. Rev. Biochem. Mol. Biol. 46*, 67−88.
(5) Rockwell, N. C., and Lagarias, J. C. (2010) A brief history of phytochromes. *ChemPhysChem 11*, 1172−1180.
(6) Song, C., Psakis, G., Lang, C., Mailliet, J., Gartner, W., Hughes, J., and Matysik, J. (2011) Two ground state isoforms and a chromophore D-ring photoflip triggering extensive intramolecular changes in a canonical phytochrome. *Proc. Natl. Acad. Sci. U.S.A. 108*, 3842−3847.
(7) Yang, X., Ren, Z., Kuk, J., and Moffat, K. (2011) Temperature-scan cryocrystallography reveals reaction intermediates in bacteriophytochrome. *Nature 479*, 428−432.
(8) Ikeuchi, M., and Ishizuka, T. (2008) Cyanobacteriochromes: A new superfamily of tetrapyrrole-binding photoreceptors in cyanobacteria. *Photochem. Photobiol. Sci. 7*, 1159−1167.
(9) Ishizuka, T., Kamiya, A., Suzuki, H., Narikawa, R., Noguchi, T., Kohchi, T., Inomata, K., and Ikeuchi, M. (2011) The cyanobacteriochrome, TepixJ, isomerizes its own chromophore by converting phycocyanobilin to phycoviolobilin. *Biochemistry 50*, 953−961.
(10) Rockwell, N. C., Martin, S. S., Feoktistova, K., and Lagarias, J. C. (2011) Diverse two-cysteine photocycles in phytochromes and cyanobacteriochromes. *Proc. Natl. Acad. Sci. U.S.A. 108*, 11854−11859.
(11) Enomoto, G., Hirose, Y., Narikawa, R., and Ikeuchi, M. (2012) Thiol-based photocycle of the blue and teal light-sensing cyanobacteriochrome Tlr1999. *Biochemistry 51*, 3050−3058.
(12) Rockwell, N. C., Martin, S. S., Gulevich, A. G., and Lagarias, J. C. (2012) Phycoviolobilin formation and spectral tuning in the DXCF cyanobacteriochrome subfamily. *Biochemistry 51*, 1449−1463.
(13) Rockwell, N. C., Martin, S. S., and Lagarias, J. C. (2012) Mechanistic insight into the photosensory versatility of DXCF cyanobacteriochromes. *Biochemistry 51*, 3576−3585.
(14) Rockwell, N. C., Martin, S. S., and Lagarias, J. C. (2012) Red/green cyanobacteriochromes: Sensors of color and power. *Biochemistry 51*, 9667−9677.
(15) Kehoe, D. M., and Grossman, A. R. (1996) Similarity of a chromatic adaptation sensor to phytochrome and ethylene receptors. *Science 273*, 1409−1412.
(16) Hirose, Y., Rockwell, N. C., Nishiyama, K., Narikawa, R., Ukaji, Y., Inomata, K., Lagarias, J. C., and Ikeuchi, M. (2013) Green/red cyanobacteriochromes regulate complementary chromatic acclimation via a protochromic photocycle. *Proc. Natl. Acad. Sci. U.S.A. 110*, 4974−4979.
(17) Hirose, Y., Shimada, T., Narikawa, R., Katayama, M., and Ikeuchi, M. (2008) Cyanobacteriochrome CcaS is the green light receptor that induces the expression of phycobilisome linker protein. *Proc. Natl. Acad. Sci. U.S.A. 105*, 9528−9533.
(18) Hirose, Y., Narikawa, R., Katayama, M., and Ikeuchi, M. (2010) Cyanobacteriochrome CcaS regulates phycoerythrin accumulation in *Nostoc punctiforme*, a group II chromatic adapter. *Proc. Natl. Acad. Sci. U.S.A. 107*, 8854−8859.
(19) Narikawa, R., Fukushima, Y., Ishizuka, T., Itoh, S., and Ikeuchi, M. (2008) A novel photoactive GAF domain of cyanobacteriochrome AnPixJ that shows reversible green/red photoconversion. *J. Mol. Biol. 380*, 844−855.
(20) Kim, P. W., Freer, L. H., Rockwell, N. C., Martin, S. S., Lagarias, J. C., and Larsen, D. S. (2012) Femtosecond photodynamics of the red/green cyanobacteriochrome NpR6012g4 from *Nostoc punctiforme*. 1. Forward dynamics. *Biochemistry 51*, 608−618.
(21) Kim, P. W., Freer, L. H., Rockwell, N. C., Martin, S. S., Lagarias, J. C., and Larsen, D. S. (2012) Second-chance forward isomerization dynamics of the red/green cyanobacteriochrome NpR6012g4 from *Nostoc punctiforme*. *J. Am. Chem. Soc. 134*, 130−133.
(22) Kim, P. W., Freer, L. H., Rockwell, N. C., Martin, S. S., Lagarias, J. C., and Larsen, D. S. (2012) Femtosecond photodynamics of the red/green cyanobacteriochrome NpR6012g4 from *Nostoc punctiforme*. 2. reverse dynamics. *Biochemistry 51*, 619−630.
(23) Lagarias, J. C., Kelly, J. M., Cyr, K. L., and Smith, W. O., Jr. (1987) Comparative photochemical analysis of highly purified 124 kDa oat and rye phytochromes in vitro. *Photochem. Photobiol. 46*, 5−13.
(24) Lamparter, T., Mittmann, F., Gartner, W., Borner, T., Hartmann, E., and Hughes, J. (1997) Characterization of recombinant phytochrome from the cyanobacterium *Synechocystis*. *Proc. Natl. Acad. Sci. U.S.A. 94*, 11792−11797.
(25) Dasgupta, J., Frontiera, R. R., Taylor, K. C., Lagarias, J. C., and Mathies, R. A. (2009) Ultrafast excited-state isomerization in phytochrome revealed by femtosecond stimulated Raman spectroscopy. *Proc. Natl. Acad. Sci. U.S.A. 106*, 1784−1789.
(26) Toh, K. C., Stojkovic, E. A., van Stokkum, I. H. M., Moffat, K., and Kennis, J. T. M. (2010) Proton-transfer and hydrogen-bond interactions determine fluorescence quantum yield and photochemical efficiency of bacteriophytochrome. *Proc. Natl. Acad. Sci. U.S.A. 107*, 9170−9175.
(27) Carroll, E. C., Compton, O. C., Madsen, D., Osterloh, F. E., and Larsen, D. S. (2008) Ultrafast carrier dynamics in exfoliated and functionalized calcium niobate nanosheets in water and methanol. *J. Phys. Chem. C 112*, 2394−2403.
(28) Larsen, D. S., Papagiannakis, E., van Stokkum, I. H. M., Vengris, M., Kennis, J. T. M., and van Grondelle, R. (2003) Excited state dynamics of $\beta$-carotene explored with dispersed multi-pulse transient absorption. *Chem. Phys. Lett. 381*, 733−742.
(29) Holzwarth, A. R. (1996) Data analysis of time-resolved measurements. In *Biophysical techniques in photosynthesis* (Amesz, J., and Hoff, A. J., Eds.) pp 75−92, Springer, Dordrecht, The Netherlands.
(30) van Stokkum, I. H. M., Larsen, D. S., and van Grondelle, R. (2004) Global and target analysis of time-resolved spectra. *Biochim. Biophys. Acta 1657*, 82−104.
(31) Freer, L. H., Kim, P. W., Corley, S. C., Rockwell, N. C., Zhao, L., Thibert, A. J., Lagarias, J., Clark, and Larsen, D. S. (2012) Chemical inhomogeneity in the ultrafast dynamics of the DXCF cyanobacteriochrome Tlr0924. *J. Phys. Chem. B 116*, 10571−10581.
(32) Burgie, E. S., Walker, J. M., Phillips, G. N., Jr., and Vierstra, R. D. (2013) A photo-labile thioether linkage to phycoviolobilin provides the foundation for the blue/green photocycles in DXCF-cyanobacteriochromes. *Structure 21*, 88−97.
(33) von Stetten, D., Gunther, M., Scheerer, P., Murgida, D. H., Mroginski, M. A., Krauss, N., Lamparter, T., Zhang, J., Anstrom, D. M., Vierstra, R. D., Forest, K. T., and Hildebrandt, P. (2008) Chromophore heterogeneity and photoconversion in phytochrome crystals and solution studied by resonance Raman spectroscopy. *Angew. Chem., Int. Ed. 47*, 4753−4755.
(34) Kaminski, S., Daminelli, G., and Mroginski, M. A. (2009) Molecular dynamics simulations of the chromophore binding site of *Deinococcus radiodurans* Bacteriophytochrome Using New Force Field Parameters for the Phytochromobilin Chromophore. *J. Phys. Chem. B 113*, 945−958.
(35) Ma, Q., Hua, H. H., Chen, Y., Liu, B. B., Kramer, A. L., Scheer, H., Zhao, K. H., and Zhou, M. (2012) A rising tide of blue-absorbing biliprotein photoreceptors: Characterization of seven such bilin-binding GAF domains in *Nostoc* sp. PCC7120. *FEBS J. 279*, 4095−4108.
(36) Spillane, K. M., Dasgupta, J., Lagarias, J. C., and Mathies, R. A. (2009) Homogeneity of phytochrome Cph1 vibronic absorption revealed by resonance Raman intensity analysis. *J. Am. Chem. Soc. 131*, 13946−13948.
(37) Larsen, D. S., van Stokkum, I. H. M., Vengris, M., van der Horst, M. A., de Weerd, F. L., Hellingwerf, K. J., and van Grondelle, R. (2004) Incoherent manipulation of the photoactive yellow protein photocycle with dispersed pump-dump-probe spectroscopy. *Biophys. J. 87*, 1858−1872.
(38) Larsen, D. S., Vengris, M., van Stokkum, I. H. M., van der Horst, M. A., de Weerd, F. L., Hellingwerf, K. J., and van Grondelle, R. (2004) Photoisomerization and photoionization of the photoactive yellow protein chromophore in solution. *Biophys. J. 86*, 2538−2550.

(39) Carroll, E. C., Song, S. H., Kumauchi, M., van Stokkum, I. H., Jailaubekov, A., Hoff, W. D., and Larsen, D. S. (2010) Subpicosecond excited-state proton transfer preceding isomerization during the photorecovery of Photoactive Yellow Protein. *J. Phys. Chem. Lett. 1*, 2793−2799.

(40) Carroll, E. C., Hospes, M., Valladares, C., Hellingwerf, K. J., and Larsen, D. S. (2011) Is the photoactive yellow protein a UV-B/blue light photoreceptor? *Photochem. Photobiol. Sci. 10*, 464−468.